

Bounding Film Drainage in Common Thin Films

by

J. E. Coons¹, P. J. Halley², S. A. McGlashan², and T. Tran-Cong³

¹*Los Alamos National Laboratory, Engineering Sciences and Applications Division, P.O. Box 1663, MS C930, Los Alamos, NM 87545, USA*

²*Centre for High Performance Polymers, School of Engineering, University of Queensland, St Lucia, QLD 4072, Australia*

³*Department of Mechanical and Mechatronic Engineering, University of Southern Queensland, Toowoomba, QLD 4350, Australia*

Submitting author: J. E. Coons, jimc@lanl.gov, +1-505-667-6362 (Phone), +1-505-665-5548 (Fax)

Abstract

A review of thin film drainage models is presented in which the predictions of thinning velocities and drainage times are compared to reported values on foam and emulsion films found in the literature. Free standing films with tangentially immobile interfaces and suppressed electrostatic repulsion are considered, such as those studied in capillary cells. The experimental thinning velocities and drainage times of foams and emulsions are shown to be bounded by predictions from the Reynolds and the theoretical MTsR equations. The semi-empirical MTsR and the surface wave equations were the most consistently accurate with all of the films considered. These results are used in an accompanying paper to develop scaling laws that bound the critical film thickness of foam and emulsion films.

Keywords: Thin Films, Thinning Velocity, Film Drainage, Scaling Law, Spontaneous Rupture

1. Introduction

Thin liquid films form between the discrete phases in multiphase systems (e.g., bubbles and droplets) and an improved understanding of their stability will benefit numerous industries relying on foam and emulsion products [1]. Several exciting applications loom on the horizon in the area of nanoscale multiphase materials, such as designed-nanostructure foams for tissue engineered constructs and soft biomedical scaffolds [2], novel market-inspired foam structures for manufactured food products and emulsions [3], and carefully designed foams for rigid structural applications in aerospace design [4]. In order to ensure that new nanoscale foam structures can be manufactured to meet the needs of the expanding variety of applications, more attention must be directed at the fundamentals of the foaming process – that is, concentrating on the basics behind thin film drainage and cell rupture mechanisms. Specifically we hope this work and the accompanying paper [5] provides a paradigm shift in the ease of prediction of the drainage and rupture of thin films. By bounding the complex dynamics in thin films, we begin to construct a framework from which insights can be made into the design of the ultimate structure and properties of market-ready nanostructured foams.

In the context of manufacturing a multiphase material with specific structural requirements, the eventual physical state of the continuous phase (e.g., the thin film) is highly influenced by the thin film drainage behavior. Despite the existence of a large body of information on the drainage of thin films, significant uncertainties remain in the ability to predict thinning velocities using basic physicochemical properties. Thin films drain as a consequence of the pressure drop between the film interior and the Plateau border at its perimeter [1, 6]. As the film thickness decreases, the intrafilm pressure increases and the flexible interfaces deform. At smaller film thicknesses, the interfaces become more corrugated and form dimples and pimples. The process in which unstable capillary waves on these interfaces become unstable and rupture the film is described in an accompanying paper [5]. Film drainage plays an important role in creating the conditions required to either maintain a stable, continuous film or create instabilities that lead to the formation of holes or film openings.

Thin film dynamics are studied in specially designed capillary cells [1]. The Scheludko cell [7] was one of the original experimental systems designed to study thin liquid films. A thin film is created in the following manner. The film medium is injected into the capillary tube until a column of liquid is obtained with concave menisci. The film medium is then removed until the menisci begin to flatten. Once the desired film radius is achieved, the thin film is allowed to drain spontaneously. Interference patterns of monochromatic light reflecting and transmitting through the thin film allow precise measurement of the film thickness. By surrounding the film with a gas or immiscible liquid, both foam [8-10] and emulsion films [9, 11] can be studied. In this paper, the thinning velocities and drainage times of thin films predicted from various drainage models are compared to experimental measurements reported in the literature. Data was selected from studies in which precautions were taken to eliminate the tangential mobility and electrostatic repulsion of the film interfaces. This was achieved by including a surfactant at or above the critical micelle concentration and a small amount of electrolyte in the film medium. The objective of this analysis is to determine if existing drainage theories accurately predict thinning velocities and drainage times of ideal films whose physicochemical properties are well known. By identifying theories that accurately predict or bound film drainage, it is possible to determine whether the conditions that lead to instability [6] and rupture [5] can be bounded.

2. Film Drainage Theory

The hydrodynamics of thin films with rigid interfaces was addressed by Reynolds [12]. Figure 1 shows a plane parallel film surrounded by a Plateau border. Application of the lubrication approximation to the Navier-Stokes equation for cylindrical thin films leads to the following Reynolds equation [6, 7, 12] for film thinning.

$$V_{\text{Re}} = -\frac{dh}{dt} = \frac{2h^3 \Delta P}{3\mu R^2} \quad (1)$$

h is the average film thickness, ΔP is the drainage pressure or average pressure drop across the film, R is the radius, t is time, V_{Re} is the (Reynolds) thinning velocity, and μ is the film viscosity. Drainage of the film occurs when the pressure within the film exceeds

that in the Plateau border. When electrostatic repulsion between the film interfaces is suppressed, the drainage pressure in the film has the following two components.

$$\Delta P = \frac{2\sigma R_c}{(R_c^2 - R^2)} + \frac{A}{6\pi h^3} \quad (2)$$

The first term on the right hand side is the capillary pressure drop due to the interfacial curvature in the Plateau border, which is the curvature of the adjacent bubble or drop menisci as affected by the presence of the film. The second term accounts for the increase in film pressure due to the attractive van der Waals forces acting between the film interfaces and is described as a negative disjoining pressure. In equation (2), A is the Hamaker constant, R_c is the radius of the capillary tube, and σ is the interfacial tension. The Hamaker constant is dependent on the materials that comprise a given film system as well as the film thickness [13]. In the following section, the equation described by Russel et al [13] is used to provide estimates of the Hamaker constant.

It has previously been shown that thin films generally exhibit faster thinning velocities than that predicted by the Reynolds equation [8, 14]. The discrepancy has been attributed to a number of factors including finite tangential mobility [15, 16], changes to the van der Waals interactions and Hamaker constant [17], the non-parallel nature of the flexible interfaces [8, 18, 19], and dynamic surface waves [20]. Attempts have been made to limit the experimental data used in this study to film systems with tangentially immobile interfaces and with known physicochemical properties. Therefore, the potential sources of enhanced thinning velocities considered here are limited to non-parallel interfacial features.

The drainage theory of Manev et al [18, 19] proposes that the intrafilm pressure increases due to the presence of hydrodynamic corrugations. Starting from a local form of the lubrication equation, Manev et al assumed that the local film thickness is a homogeneous function of the average film thickness, that the waveform driving the drainage develops by intrafilm capillary forces, and that the pressure drop across the film is proportional to the drainage pressure divided by the square root of the eigenvalue of the dominant waveform. These assumptions lead to the following expression for thinning velocity.

$$V = V_{Re} l^{3/2} \quad (3)$$

l is the number of domains or rings in the film and is given by the following theoretical expression.

$$l = \left[\frac{\Delta P}{h\sigma} \left(\frac{R}{4} \right)^2 \right]^{2/5} \geq 1 \quad (4)$$

Equations (3) and (4) are referred to here as the theoretical MTsR equation. Coons et al [6] compared the thinning velocities predicted by the theoretical MTsR equation to the experimental measurements of Radoev et al [8] and determined that the predicted velocities were consistently higher than the experimental measurements. By plotting the velocity ratio [i.e., $(V_{\text{Measured}}/V_{\text{Re}})^{2/3}$] against the theoretical number of domains from equation (4), the following semi-empirical expression for l was obtained.

$$l = \frac{1}{2} \left\{ \left[\frac{\Delta P}{h\sigma} \left(\frac{R}{4} \right)^2 \right]^{2/5} + \frac{4}{3} \right\} \geq 1 \quad (5)$$

Equations (3) and (5) are referred to here as the semi-empirical MTsR equation. Equations (4) and (5) indicate that thick films drain in accordance with the Reynolds equation down to a specific film thickness. The point of departure can be referred to as the Reynolds film thickness [6]. As the film thickness decreases below the Reynolds thickness, the number of domains increases above unity and the thinning velocity exceeds that predicted by the Reynolds equation. A comparison of equations (4) and (5) reveals that the semi-empirical equation for l provides a slightly larger Reynolds thickness than the purely theoretical form. Also, the number of domains given by the semi-empirical equation is less than that given by the theoretical equation when the theoretical number of domains exceeds 4/3. As this crossover point is often exceeded, the semi-empirical MTsR equation generally provides lower thinning velocities than the theoretical MTsR equation.

The drainage models described thus far were developed under the assumption that hydrodynamic corrugations are static waves superimposed onto a plane parallel interface. Ruckenstein and Sharma [20] hypothesized that hydrodynamic corrugations traverse the

film laterally and induce a pumping action. The following surface wave equation was derived to predict the effect of the hypothetical pumping on the film thinning velocity.

$$V = V_{Re} \left[1 + 7.35 \left(\frac{R}{R_\varepsilon} \right) \left(\frac{2\varepsilon}{h} \right) \right] \quad (6)$$

ε is the amplitude of the hydrodynamic corrugations on a single interface and R_ε is the film radius at which ε becomes negligible, which is not generally known or reported in experimental studies. Radoev et al [8] observed that ε is independent of film thickness and a strong function of film radius. Sharma and Ruckenstein [21] provide a simple equation to estimate ε based on the film radius, but this is only applicable for the film systems studied by Radoev et al. Tsekov [19] derived a film thickness dependent expression for ε , but did not identify a non-arbitrary reference thickness to determine the exact form of the dependency. Coons et al [6] explored the dependency of ε at the lower limit of the maximum transition thickness, which is a non-ambiguous reference thickness, and determined the following correlation.

$$\varepsilon = \frac{75.9 \zeta_0 B^*}{B^* + 8.57} \quad (7)$$

B^* is a dimensionless number that is dependent on the fundamental physicochemical properties of the film (see reference [6] for the method of calculation). In this study, equation (7) was also used to estimate R_ε after setting ε equal to ζ_0 , the initial amplitude of the thermal corrugation estimated from the following expression [8].

$$\zeta_0 = \sqrt{k_B T / \sigma} \quad (8)$$

k_B is Boltzmann's constant (1.38054×10^{-23} Nm/°K) and T is absolute temperature. R_ε was found to be a function of two dimensionless parameters, A^* and P_ε^* . Over the $[A^*, P_\varepsilon^*]$ range of interest $[0.1-10, 10^2-10^{18}]$, R_ε is given by the following scaling law.

$$R_\varepsilon = 2.224 \zeta_0 (P_\varepsilon^*)^{0.692} (A^*)^{-3.697} \quad (9)$$

$$A^* = \left(\frac{A}{4\pi\alpha_{0,1}^2 k_B T} \right)^{1/4} \quad (10)$$

$$P_\varepsilon^* = \frac{A}{6\pi(2\zeta_0)^3} \left(\frac{R_c}{2\sigma} \right) \quad (11)$$

$\alpha_{0,1}$ has a value of 2.4048 and is the first root of the Bessel function of first kind order zero. Equation (9) allows R_ε to be estimated from the temperature, interfacial tension, Hamaker constant, and radius of the capillary tube. Radoev et al extrapolated their ε measurements to estimate R_ε as 50 μm . Using the properties shown in Table 1, equation (9) provides R_ε values less than 26 μm . Having described the drainage models and their dependencies, the method used to estimate the Hamaker constant is presented next.

3. Hamaker Constant Approximation

The drainage theories described in the previous section are dependent on the Hamaker constant, which in turn is dependent on the dielectric spectrum of the materials in the specific film system as well as the film thickness. For all of the films used in this review, equation 5.9.3 in Russel et al [13] was used to estimate the Hamaker constant.

$$A_{131} \approx \frac{3}{4} k_B T \left[\frac{\varepsilon_1(0) - \varepsilon_3(0)}{\varepsilon_1(0) + \varepsilon_3(0)} \right]^2 + \frac{3\hbar\omega_3}{16\sqrt{2}} \left[\frac{(n_1^2 - n_3^2)^2}{(n_1^2 + n_3^2)^{1.5}} \right] \left[\frac{1}{1 + \left(\pi h \omega_3 n_3 \sqrt{n_1^2 + n_3^2} / 4c\sqrt{2} \right)^{1.5}} \right]^{2/3} \quad (12)$$

The subscript on the Hamaker constant is absent in the previous section and denotes a film of material 3 with semi-infinite material 1 at each interface. c is the speed of light (2.9979 $\times 10^8$ m/s), h is the average film thickness of material 3, \hbar is Planck's constant (1.0545 $\times 10^{-34}$ Nms/radian), n_i is the refractive index in the visible frequency range of material i , $\varepsilon_i(0)$ is the static dielectric constant of material i , and ω_3 is the dominant relaxation frequency (rad/s) of material 3 in the ultraviolet frequency range. The material specific properties are dependent on temperature. The refractive index is also dependent on the wavelength in the visible range. Hough and White [22] describe a method employing a Cauchy plot in which the refractive index through the visible range is used to determine the appropriate relaxation frequency and refractive index for a given material. This method was employed to obtain n and ω when values could not be found in the literature.

When the film material is highly polar (e.g., water), electrolytes are added to suppress the electrostatic repulsion that develops between the interfaces. The presence of ions in the film material effectively screens out the nonretarded term (i.e., the first term on the right hand side in equation (12)) when the film thickness is a few times larger than the Debye screening length [23]. The screening effect was applied when electrolytes were present in material 3 (i.e., the film material) by multiplying the nonretarded term by the following expression.

$$(2\kappa h)e^{-2\kappa h} \quad (13)$$

κ is the inverse of the Debye screening length, which for aqueous films containing +1 and -1 charged electrolytes (e.g., NaCl) was estimated from the following expression [23].

$$\kappa = \frac{M_{salt}^{1/2}}{3.04 \times 10^{-9}} \left(\frac{298.15^\circ K}{T} \right)^{1/2} \quad (14)$$

M_{salt} is the molar salt concentration and κ has a unit of meter⁻¹. A more thorough description of equations (12) and (13) can be found in Russel et al [13] and Israelachvili [23], respectively.

The dielectric and optical properties used to calculate the Hamaker constants, and when available their temperature dependencies, are provided in Table 2. Ion concentrations and the Hamaker constants used to predict thinning velocities are provided in Table 1. Having presented the drainage theories, the required physicochemical properties, and the methods used to estimate the various constants, it is now possible to compare model predictions with the experimental measurements reported in the literature

4. Results and Discussion

Thinning velocities have been reported in very few thin film studies. Radoev et al [8] reported thinning velocities in aqueous foam films at specified minimum film thicknesses, where the minimum film thickness is defined as:

$$h_{min} = h_{avg} - 2\epsilon \quad (15)$$

ϵ is the amplitude of the hydrodynamic corrugations. In order to predict thinning velocities, the average film thickness for each film was estimated using the amplitude correlation

provided by Sharma and Ruckenstein [21] in equation (15). The average thinning velocity amongst films of identical radius was calculated and compared to the average of the experimentally measured thinning velocities in Figure 3. None of the film drainage models consistently predict accurate velocities over the entire range of radii. The most accurate thinning velocities for films of radius 100 microns or less are provided by the semi-empirical MTsR equation and the surface wave equation. The accuracy of the semi-empirical MTsR equation is not coincidental as the equation parameters were obtained from a least square fit to this data [6]. For films with radii between 100 and 200 microns, the accuracy of the theoretical MTsR equation is comparable to that of the semi-empirical MTsR and surface wave equations. For larger films, the semi-empirical MTsR equation provides the most accurate thinning velocities. The measured velocities are consistently larger than the predictions of the Reynolds equation and smaller than the predictions of the theoretical MTsR equation, the latter providing about twice that of the measured velocities.

Rao et al [15] reported thinning velocities for aqueous foam films of similar size, but the velocities are several orders of magnitude higher than those reported by Radoev et al [8]. For a film of radius 90 microns, Rao et al report thinning velocities between 2000 and 5000 Å/sec at a film thickness of 400 Å and Radoev et al report a thinning velocity of 7.1 Å/sec at a film thickness of 294 Å. Using the film thickness and drainage pressure dependency of the Reynolds equation to adjust the thinning velocity of Radoev et al to 400 Å results in an estimated 8.7 Å/sec, which is still orders of magnitude lower than the range reported by Rao et al. A discrepancy of this magnitude can only be explained by a reporting error in the data of Rao et al. Therefore, the thinning velocities of Rao et al are not considered further.

As a consequence of the rarity of thinning velocity measurements reported in the literature, film drainage times were also collected. Theoretical drainage times were calculated by integrating between the stipulated initial and final film thickness according to the following equation:

$$\Delta t = \int_{h_{low}}^{h_{high}} \frac{dh}{V} \quad (16)$$

V is given by equations (1), (3), or (6), h_{high} is the average film thickness at the initial condition, and h_{low} is the average film thickness at the final condition. Integration of equation (16) was performed numerically using the DQDAG subroutine from the IMSL library, while incorporating the film thickness dependency of the Hamaker constant. However, it was determined that carefully fixing the value of the Hamaker constant throughout the integration also provided accurate drainage times. This is due to the relatively low contribution of the disjoining pressure over the thickness range considered. As shown by the dashed curves in Figure 2, the disjoining pressure component does not contribute significantly to the drainage pressure until approximately 500 Å, which is near the lower film thickness limit of the drainage time integral. By fixing the Hamaker constant to the value at the lower thickness limit, the resulting drainage times were found to be accurate to within one percent, except for those determined from the surface wave model. In the latter case, the Hamaker constant plays a somewhat larger role in determining the deviation from Reynolds flow. Consequently, drainage times determined from the surface wave model with a fixed (larger) Hamaker constant were 5 to 20% lower, with the largest effect obtained for the large radii films. Although not shown here, the drainage times calculated with the fixed Hamaker constant were generally closer to the measured value. For this reason, the Hamaker constant shown in Table 1 is the value corresponding to the Hamaker constant at the lower thickness limit of the drainage time integral.

Manev et al [9] and Kumar et al [10] reported drainage times for aqueous foam films. Manev et al measured drainage times as a function of surfactant and electrolyte concentration as the films thinned from 2000 to 500 Å in thickness. The ratio of theoretical to experimental drainage times are compared in Figure 4, plots (a) through (d). The semi-empirical MTsR and surface wave equations are most accurate with foam films of radius greater than 100 μm, whereas the Reynolds equation is most accurate for smaller films. Drainage times determined from the theoretical MTsR equation are typically about half of the measured value. Drainage times for the plane-parallel film of Kumar et al are presented in Table 3, where the theoretical and semi-empirical MTsR equations are shown to be most

accurate. The drainage times for all of the foam films measured by Manev et al and Kumar et al are bounded by the Reynolds equation and the theoretical MTsR equation.

Drainage times of emulsion films were measured by Traykov et al [11] and Manev et al [9]. Drainage times reported by Traykov et al for films of 100 μm radius are compared to the predictions from theory in Table 3 and those of Manev et al are compared in Figure 4, plots (e) and (f). As with the foam films, the semi-empirical MTsR and the surface wave equations provide the most accurate predictions of drainage times, particularly for emulsion films with a radius greater than 100 μm . The Reynolds and surface wave equations are more accurate for emulsion films of radii smaller than 100 μm . Drainage times determined from the theoretical MTsR equation are typically about half of the measured value. The drainage times measured by Traykov et al and Manev et al are bounded by the Reynolds and the theoretical MTsR equations.

5. Conclusions

An analysis of film drainage is provided in which thinning velocities and drainage times predicted by existing drainage theories are compared to reported measurements from foam and emulsion thin film experiments. Approximate correlations for previously undefined model parameters (i.e., the amplitude of the hydrodynamic corrugations and the film radius at which the amplitudes become significant) are provided as functions of fundamental film properties. The thinning velocity and drainage times of all of the foam and emulsion films were bounded by the Reynolds equation and the theoretical MTsR equation. The Reynolds equation was typically the most accurate predictor of drainage times of all films less than 100 μm in radius, whereas the semi-empirical MTsR equation provided the most accurate drainage times over the entire span of film sizes. Accuracy of the semi-empirical MTsR equation with the data of Radoev et al is expected as the model parameters were obtained by a fit to the data [6]. Thinning velocities predicted by the theoretical MTsR equation were generally about twice as large as the measured value, resulting in drainage times that were about half of the measured values. These results are used in an accompanying paper [5] to develop scaling laws that bound the critical rupture thickness of foam and emulsion films.

5. Acknowledgements

This work was supported in part by the U. S. Department of Energy under contract W-7405-ENG-36.

6. References

1. I.B. Ivanov and D.S. Dimitrov, *Thin Film Drainage*, Marcel Dekker, Inc., 1988.
2. D.W. Hutmacher, M. Sittinger and M.V. Risbud, *Trends in Biotechnology*, 22 (2004) 354
3. P. Wilde, A. Mackie, R. Husband, P. Gunning and V. Morris, *Adv. Colloid Interface Sci.*, 108-09 (2004) 63
4. E.S. Weiser, T.F. Johnson, T.L. St Clair, Y. Echigo, H. Kaneshiro and B.W. Grimsley, *High Performance Polymers*, 12 (2000) 1
5. J.E. Coons, P.J. Halley, S.A. McGlashan and T. Tran-Cong, *Colloid Surf. A-Physicochem. Eng. Asp.*, (Submitted 2004)
6. J.E. Coons, P.J. Halley, S.A. McGlashan and T. Tran-Cong, *Adv. Colloid Interface Sci.*, 105 (2003) 3
7. A. Sheludko, *Adv. Colloid Interface Sci.*, 1 (1967) 391
8. B.P. Radoev, A.D. Scheludko and E.D. Manev, *J. Colloid Interface Sci.*, 95 (1983) 254
9. E.D. Manev, S.V. Sazdanova and D.T. Wasan, *J. Colloid Interface Sci.*, 97 (1984) 591
10. K. Kumar, A.D. Nikolov and D.T. Wasan, *J. Colloid Interface Sci.*, 256 (2002) 194
11. T.T. Traykov, E.D. Manev and I.B. Ivanov, *International Journal of Multiphase Flow*, 3 (1977) 485
12. O. Reynolds, *Philos. Trans. R. Soc. London*, 177 (1886) 157
13. W.B. Russel, D.A. Saville and W.R. Schowalter, *Colloidal Dispersions*, Cambridge University Press, New York, 1989.
14. E. Manev and R.J. Pugh, *J. Colloid Interface Sci.*, 186 (1997) 493
15. A.A. Rao, D.T. Wasan and E.D. Manev, *Chem. Eng. Commun.*, 15 (1982) 63
16. B.P. Radoev, D.S. Dimitrov and I.B. Ivanov, *Colloid and Polymer Science*, 252 (1974) 50

17. E. Manev, A. Scheludko and D. Exerowa, *Colloid and Polymer Science*, 252 (1974) 586
18. E. Manev, R. Tsekov and B. Radoev, *J. Dispersion Sci. Technol.*, 18 (1997) 769
19. R. Tsekov, *Colloid Surf. A-Physicochem. Eng. Asp.*, 141 (1998) 161
20. E. Ruckenstein and A. Sharma, *J. Colloid Interface Sci.*, 119 (1987) 1
21. A. Sharma and E. Ruckenstein, *Langmuir*, 3 (1987) 760
22. D.B. Hough and L.R. White, *Adv. Colloid Interface Sci.*, 14 (1980) 3
23. J.N. Israelachvili, *Intermolecular and Surface Forces*, Academic Press, San Diego, 1992.
24. R.C. Weast, *Handbook of Chemistry and Physics*, CRC Press, Inc., Boca Raton, FL, 1983.
25. M. Debenham and G.D. Dew, *Journal of Physics E: Scientific Instruments*, 14 (1981) 544

Tables

Table 1. Physicochemical Properties of the Film Systems.

Reference	Film Type	$A \times 10^{20}$ (Nm)	T (°C)	$\sigma \times 10^3$ (N/m)	$\mu \times 10^3$ (Ns/m)	R_c (μm)	R (μm)	$h_{high} - h_{low}$ (Å)
Radoev et al [8]	Foam ¹	1.41	24	34.5	0.89	1790 ²	50	-
	"	1.36	"	"	"	"	60	-
	"	1.29	"	"	"	"	65	-
	"	1.26	"	"	"	"	70	-
	"	1.30	"	"	"	"	75	-
	"	1.26	"	"	"	"	80	-
	"	1.23	"	"	"	"	90	-
	"	1.17	"	"	"	"	100	-
	"	1.13	"	"	"	"	115	-
	"	1.13	"	"	"	"	150	-
	"	0.97	"	"	"	"	200	-
	"	0.79	"	"	"	"	500	-
	"	0.75	"	"	"	"	700	-
"	0.68	"	"	"	"	1000	-	
<hr/>								
Manev et al [9]								
No. 1	Foam ³	0.79	25	44.5	0.89	1790	50-500	2000-500
No. 2	Foam ⁴	"	"	37.0	"	"	"	"
No. 3	"	"	"	34.0	"	"	"	"
No. 4	"	"	"	34.0	"	"	"	"
No. 5	Emulsion ⁵	0.12	"	15.0	"	1580	50-300	"
No. 6	Emulsion ⁶	"	"	7.9	"	"	"	"
<hr/>								
Traykov et al [11]								
No. 1	Emulsion ⁷	0.36	20	28.0	1.0	1350	100	1600-840
No. 4	Emulsion ⁸	0.10	"	34.0	"	1450	"	"
<hr/>								
Kumar et al [10]	Foam	0.41	25	37.1	0.89	930	178	4000-1020

¹ Aqueous films contained 0.1M NaCl.

² Not reported in reference but estimated from the reported capillary pressure drop.

³ Aqueous films contained 0.1M NaCl.

⁴ Aqueous films contained 0.25M NaCl.

⁵ Toluene in water (o/w) emulsion. The aqueous films contained 0.3M NaCl..

⁶ Toluene in water (o/w) emulsion. The aqueous films contained 0.1M NaCl.

⁷ Water in benzene (w/o) emulsion.

⁸ Benzene in water (o/w).emulsion. The aqueous films contained 0.3M NaCl.

Table 2. Dielectric and optical properties⁹ of reference film materials.

Material	$\epsilon(0)$	n	$\omega \times 10^{-16}$ (rad/s)
water	$10^{-0.002(T-298.15)+\log_{10}(78.54)}$	1.333	1.88
air	1.00054	1	-
benzene	$2.284 - .002(T - 293.15)$	1.5011	1.32
toluene	$2.379 - .00243(T - 298.15)$	1.474	1.36

⁹ $\epsilon(0)$ were obtained from Weast [24]. n and ω for water and benzene were obtained from Israelachvili [23]. n and ω for toluene were obtained from a Cauchy plot prepared using the refractive index data reported by Debenham and Dew [25].

Table 3. Experimental and Theoretical Drainage Times of Thin Films

Reference	Film Type	Δt_{exp} (s)	Δt_{theory} (s)			
			Reynolds Equation	Semi-Empirical MTsR	Theoretical MTsR	Surface Wave Equation
Kumar et al [10]	Foam	4.0	23.0	5.6	3.1	6.5
Traykov et al [11]	Emulsions					
	No. 1	10.8	18.4	7.3	5.1	10.6
	No. 4	8.9	16.3	6.7	4.7	12.6

Figure Captions

Figure 1. The formation and drainage of a free-standing thin film in a capillary cell. Deviations from the ideal plane-parallel interfaces include large scale hydrodynamic corrugations such as the dimples that have formed in the film on the far right.

Figure 2. Calculated Hamaker constants over the film thickness range of interest are provided by the solid curves for: (a) air-water-air foam films of Radoev et al [8], Manev et al [9] (Nos. 1 through 4), and Kumar et al [10], (b) toluene-water-toluene emulsion (O/W) films of Manev et al [9] (Nos. 5 and 6), (c) water-benzene-water emulsion (W/O) films of Traykov et al [11] (No. 1), and (d) benzene-water-benzene emulsion (O/W) films of Traykov et al [11] (No. 4). The dashed curves provide the ratio of the disjoining pressure to the Plateau border pressure drop that make up the film drainage pressure.

Figure 3. The ratio of theoretical to measured drainage velocity for the films of Radoev et al [8]. All experimental measurements are bounded by the Reynolds equation and the theoretical MTsR equation. Theoretical results are indicated for the Reynolds equation (\circ), the semi-empirical MTsR equation (Δ), theoretical MTsR equation (\square), and the surface wave equation (\times).

Figure 4. The ratio of theoretical to measured drainage times for the films of Manev et al [9]. Plots (a) through (d) refer to foam films Nos. 1 through 4, respectively. Plots (e) and (f) refer to emulsion films Nos. 5 and 6, respectively. Theoretical results are indicated for the Reynolds equation (\circ), the semi-empirical MTsR equation (Δ), theoretical MTsR equation (\square), and the surface wave equation (\times).

Figures

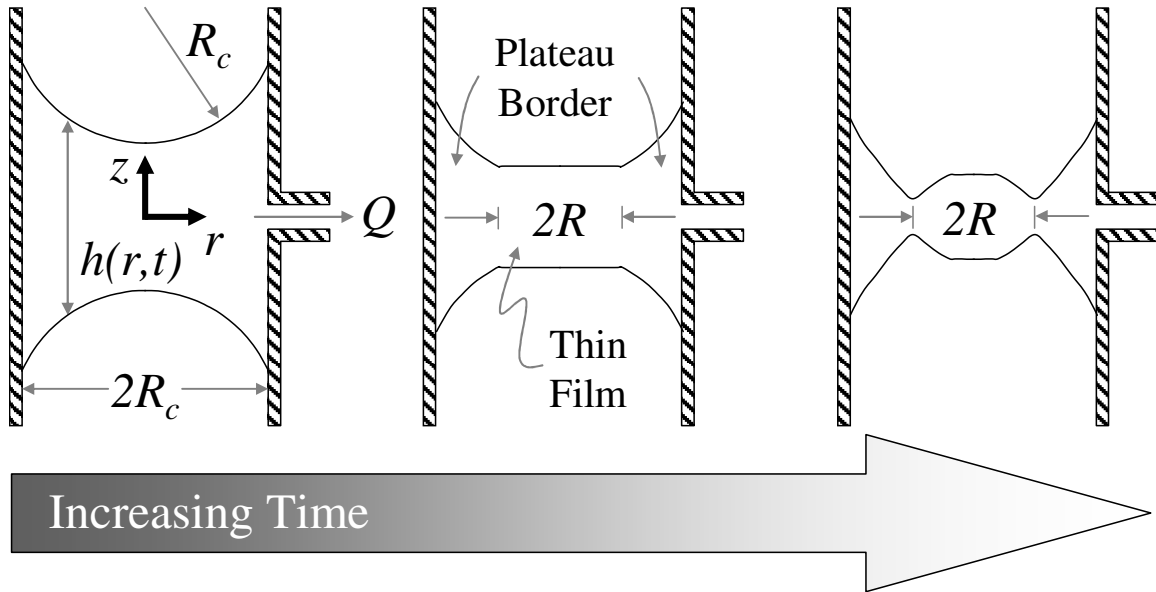


Figure 1.

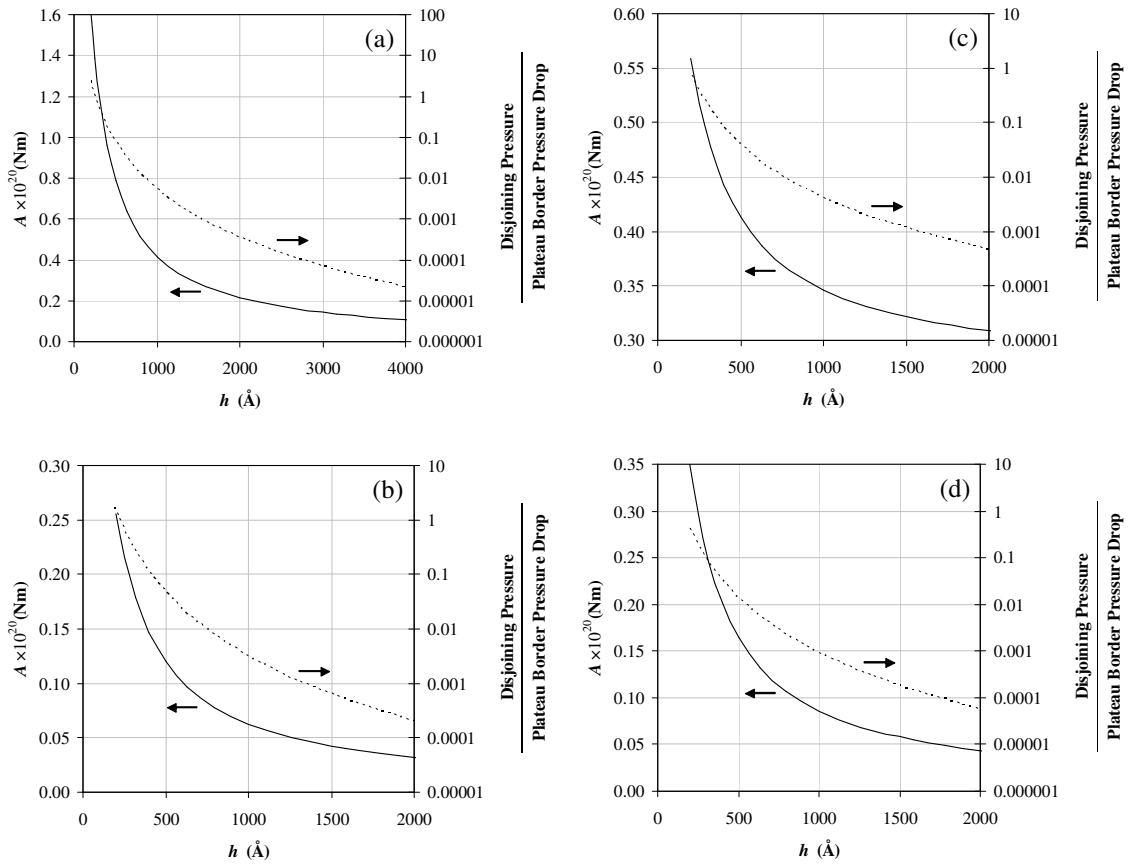


Figure 2.

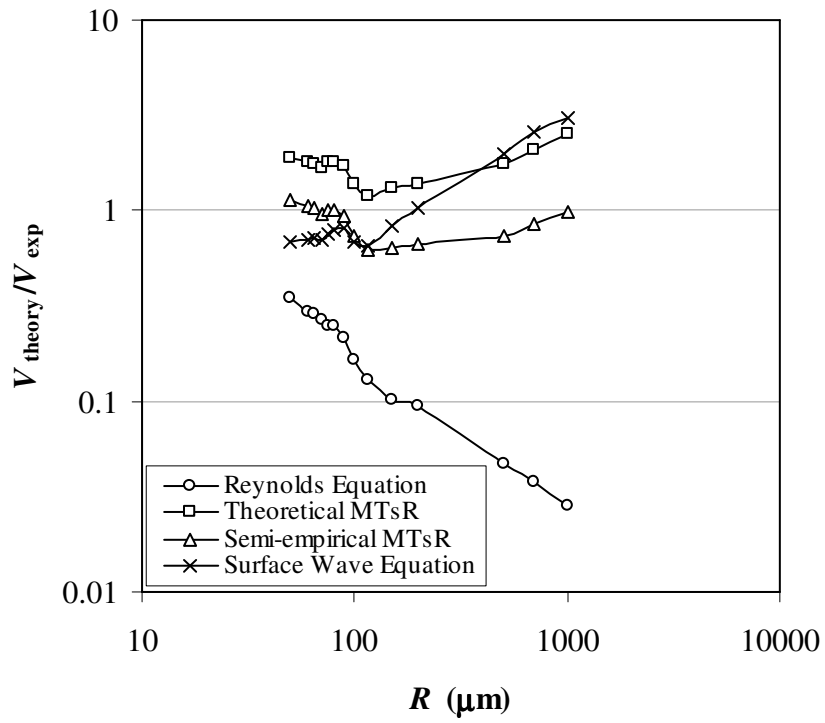


Figure 3.

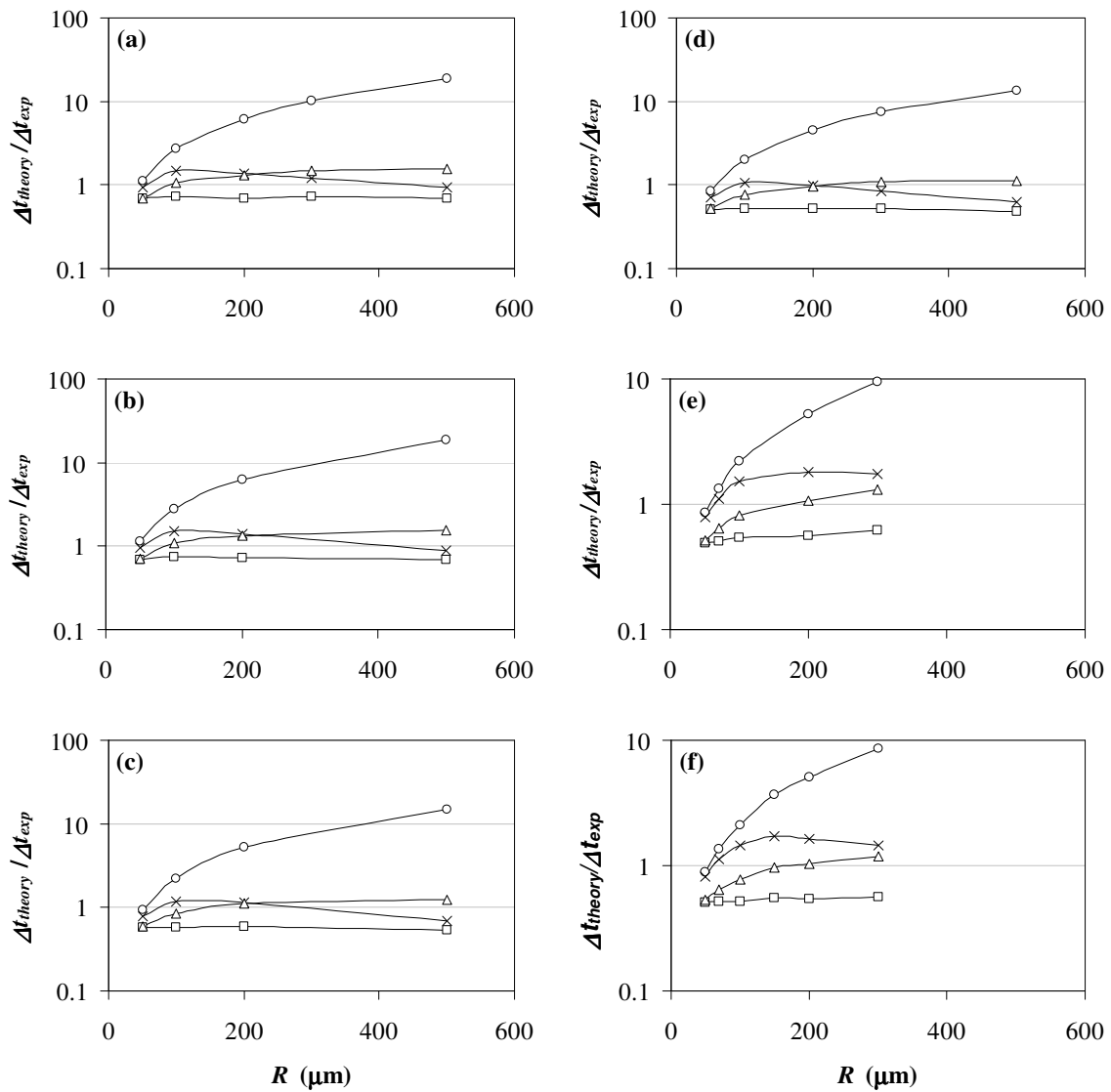


Figure 4.